Observing Nucleation Close to the Binodal by Perturbing Metastable Polymer Blends

A. J. Patel[†] and N. P. Balsara*[,†,‡]

Department of Chemical Engineering, University of California, Berkeley, California 94720, and Materials Sciences Division and Environmental Energy Technologies Division, Lawrence Berkeley National Laboratory, University of California, Berkeley, California 94720

Received August 22, 2006; Revised Manuscript Received November 19, 2006

ABSTRACT: The initial stages of liquid−liquid phase separation in an off-critical binary polymer blend were studied by time-resolved small-angle neutron scattering (SANS). Phase separation is triggered by quenching homogeneous blends from the single-phase to the two-phase region of the phase diagram. Our objective was to determine the size of the critical nucleus, R_c, over a wide range of quench depths, κ. We present results obtained from two-step quenches. In the first step, the blend is subjected to a deep quench, κ', for a brief period of time. This is followed by a reduction in quench depth to κ. One can view the first quench as a perturbation. We demonstrate that under certain conditions the only effect of the perturbation is to hasten nucleation kinetics at κ. This allows the determination of R_c at low quench depths near the binodal, where nucleation barriers preclude the formation of viable nuclei after single-step quenches on experimental time scales. Our experiments at large κ provide no evidence for a change in phase separation mechanism upon crossing the classical spinodal.

Introduction

Predicting the kinetics of commonly observed phase transitions such as boiling, crystallization, and liquid−liquid phase separation from first principles remains an important unresolved scientific challenge.[1−14] These first-order phase transitions are characterized by free energy barriers (ΔG_N) that prevent the spontaneous formation of the new phase. Classical nucleation theory assumes that this barrier is crossed by the formation of nuclei that are larger than a certain critical size (R_c). It is assumed that the size of the nucleus (R) is the relevant "reaction coordinate" for describing nucleation, and the typical dependence of ΔG_N on R is shown in Figure 1. ΔG_N is peaked at $R = R_c$, and the peak height gives the magnitude of the nucleation barrier. Both the barrier height and R_c increase with decreasing quench depth, κ, and tend to infinity as the binodal (coexistence curve) is approached. For the present purposes, quench depth is defined as the "thermodynamic distance" between the coexistence curve and metastable state of interest.[15] The time scale for the formation of a critical nucleus increases sharply near the binodal, making experimental observation difficult.

In previous studies,[10,16−20] we have shown that the initial stages of nucleation in metastable polyolefin blends can be studied by time-resolved small-angle neutron scattering (SANS). Phase separating polyolefin blends are ideally suited for investigating the initial stages of nucleation[17] because: (1) The equilibrium properties of the polymer blend are in excellent agreement with the predictions of the Flory−Huggins theory. This enables quantitative predictions of the dependence of R_c on quench depth. (2) Nucleating clusters can readily be detected by scattering techniques due to the large molecular size. (3) Because of entanglement effects, the kinetics of nucleation are slow and can thus be readily tracked by time-resolved measurements.

In all nucleation studies, the range of conditions over which nucleation kinetics can be measured depends on experimental limitations. The upper limit of quench depth is determined by the shortest time scale, and the smallest length scale that can be resolved by the experiment. In this paper we show that there is essentially no upper limit for the quench depth that can be studied in our system. In other words, the kinetics of nucleation at very large quench depths and the size of the nuclei found in this regime are well within experimental resolution. The lower limit of quench depth is determined by the longest possible experiment that can be conducted and the largest length scale that can be resolved experimentally. In this paper, we demonstrate a method for extending the lower limit of the quench depth where nucleation can be observed. We do this by imposing carefully designed perturbations on the metastable systems.

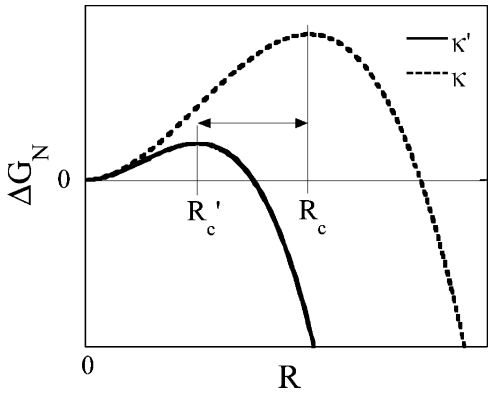

Figure 1. Classical nucleation theory predictions for the change in free energy for the formation of a nucleus of size R (qualitative plots) for different quench depths κ and κ' ($\kappa < \kappa'$).

In Figure 1, we show $\Delta G_N(R)$ curves for two hypothetical quench depths κ' and κ; $\kappa < \kappa'$. Direct quenches from a stable state to metastable states with quench depths κ and κ' would lead to the formation of critical nuclei of sizes R_c and R_c' ($R_c' < R_c$), respectively, as shown in Figure 1. Our interest is in two-step quenches wherein the system is first quenched to κ' for a brief period of time and then quenched to κ. One can view the first quench as a perturbation. By comparing the results obtained from single-step and two-step quenches to κ, we will study the effect of this perturbation on the nucleation process at quench depth κ. The first quench to κ' will breed a population

[†] Department of Chemical Engineering.
[‡] Lawrence Berkeley National Laboratory.

10.1021/ma061947+ CCC: $37.00
Published on Web 02/02/2007

of nuclei with sizes $R > R_c'$. Some of these nuclei, $R_c' < R < R_c$, are, however, not viable during the second quench to κ. If the time spent at κ' is sufficiently small and the extent of phase separation during this step is limited, then we expect to observe the dissolution of nuclei with $R_c' < R < R_c$ during the second quench. Our objective is to design experiments where the perturbative quench to κ' only hastens nucleation at κ. In such an experiment, the concentration of critical nuclei after the two-step quench would eventually be identical to that obtained after a direct quench to κ. Beyond this stage, one could apply methods developed for analyzing direct quench experiments[10,19] to determine R_c. We use this approach to determine R_c at small κ values where activation barriers are large, and nucleation after single-step quenches does not occur on experimentally viable time scales.

Experimental Section[42]

We have studied an off-critical, binary blend of high molecular weight liquid polyolefins, deuterated polymethylbutylene (*d*PMB) and hydrogenous polyethylbutylene (*h*PEB). The methods used to synthesize and characterize these nearly monodisperse homopolymers are described in refs 21 and 22. The weight-average molecular weights are 153 kg/mol (*d*PMB) and 197 kg/mol (*h*PEB). The radii of gyration of both chains are 15.4 ± 1.0 nm. On average, there are 4.5 deuterium atoms for every five carbon atoms in *d*PMB. The results reported here are from a blend with *d*PMB volume fraction, $\phi_{d\mathrm{PMB}} = 0.20$. Our polymers are much larger than the threshold for chain entanglement.[23]

The blend was studied by small-angle neutron scattering (SANS) on the NG3 beamline at the National Institute of Standards and Technology (NIST) in Gaithersburg, MD. The blends were housed in the NIST pressure cell, capable of controlling pressure (P) and temperature (T) in the $0.03 < P < 3.10$ kbar and $30 < T < 200$ °C range. The azimuthally averaged coherent scattering intensity, I, as a function of the magnitude of the scattering vector, q [$q = (4\pi/\lambda)\sin(\theta/2)$, where θ is the scattering angle and λ is the wavelength of the incident neutrons], was obtained by methods reported in ref 21. Static SANS enabled the thermodynamic characterization of our system, while time-resolved SANS enabled the study of nucleation.

We report the results from two types of quench experiments: single-step and two-step quenches. In the past, we have reported extensively on the results from single-step quench experiments.[10,17−20] This is the traditional nucleation experiment wherein a sample in the stable one-phase region is quenched into the two-phase region by an increase in pressure. In the two-step quench experiments, we quench the system to a quench depth, κ', wait for a certain amount of time, τ_1, and then carry out the second step, by reducing the quench depth of the sample to κ. Isothermal pressure quenches, executed in less than 2 min, were used to quench the sample from one state to the other.

Theoretical Framework

The SANS intensity from a polymer blend at a given temperature and pressure is

$$I(q;t) = (b_1/v_1 - b_2/v_2)^2 S(q;t) \tag{1}$$

where b_i is the neutron scattering length of a monomer in polymer chain i with a monomer volume v_i, and $S(q;t)$ is the static structure factor of the blend at time t after the initiation of the quench from the homogeneous one-phase region.

For a homogeneous blend, the time-independent static structure factor is given by the random phase approximation (RPA)[24]

$$S_{\mathrm{RPA}}(q) = [(N_1 v_1 \phi_1 P_1(q))^{-1} + (N_2 v_2 \phi_2 P_2(q))^{-1} - 2\chi/v_0]^{-1} \tag{2}$$

where χ is the Flory−Huggins interaction parameter, N_i is the number of monomer units with volume v_i in polymer chain i, v_0 is a reference volume (here 100 Å^3), ϕ_i is volume fraction of polymer i, and $P_i(q)$ is the corresponding Debye function

$$P_i(q) = [2/x^2][e^{-x} + x - 1] \tag{3}$$

where $x = q^2 R_{gi}^2$. $R_{gi}^2 = \alpha N_i l_{i,\mathrm{ref}}^2/6$, where $l_{i,\mathrm{ref}}$ is the statistical segment length at a reference pressure and temperature of 25 °C and 0.1 MPa determined for PMB and PEB chains in ref 21. In the RPA analysis of the static SANS profiles, χ and α are used as the fitting parameters.[25] (The statistical segment length obtained from our fits are typically within 10% of the literature values.)

Knowledge of the temperature and pressure dependencies of χ permits a complete thermodynamic description of the blend using the Flory−Huggins theory,[26−28] where the free energy density of mixing (G_m) is

$$\beta G_m = [\phi_1 \ln \phi_1/(v_1 N_1)] + [(1 - \phi_1)\ln(1 - \phi_1)/(v_2 N_2)] + [\chi(T,P)\phi_1(1 - \phi_1)/v_0] \tag{4}$$

where $\beta = 1/k_B T$ and k_B is the Boltzmann constant. The binodal is found by equating the chemical potentials between phases, $\mu_1^{\mathrm{I}} = \mu_1^{\mathrm{II}}$ and $\mu_2^{\mathrm{I}} = \mu_2^{\mathrm{II}}$, where the superscripts denote phase I or II and the subscripts refer to the components of the blend. Within the Flory−Huggins framework, the spinodal or the limit of metastability is unambiguously defined for a given temperature and pressure (below the critical point) as the locus of inflection points of the function $G_m(\phi_1)$.[29,30]

We define a normalized quench depth κ as

$$\kappa(T,P;\phi_1) = \frac{\chi(T,P) - \chi_b}{\chi_s - \chi_b} \tag{5}$$

where χ_b is the value of the Flory−Huggins interaction parameter at the binodal and χ_s is its value at the spinodal. Our quench depth is thus normalized to be 0 at the binodal and 1 at the spinodal.

Results and Discussion

In order to obtain $\chi(T,P)$, we perform static SANS measurements in the homogeneous one-phase region and then use the random phase approximation (eqs 1−3) to fit the scattering profiles. Using $\chi(T,P)$ thus obtained and using the Flory−Huggins theory, we can obtain the binodal and spinodal curves as described in the previous section. These curves for our *d*PMB/*h*PEB blend with $\phi_{d\mathrm{PMB}} = 0.20$ are shown in a T vs P phase diagram in Figure 2. The methods and parameters used to determine this diagram are given in ref 31 and summarized in Table 1. The symbols in Figure 2 indicate the conditions under which phase separation was studied; the diamonds show the location of the single-step quenches while the squares show the final step of the two-step quenches. The values of κ for each of the quench conditions shown in Figure 2 are listed in Table 2. Note that there are a number of metastable states that were studied both by single-step and two-step quenches.

Prior to each experiment, the blend was homogenized in the one-phase regime at $T = 86.5$ °C and $P = 0.03$ kbar. The blend was then cooled isobarically to the desired quench temperature,

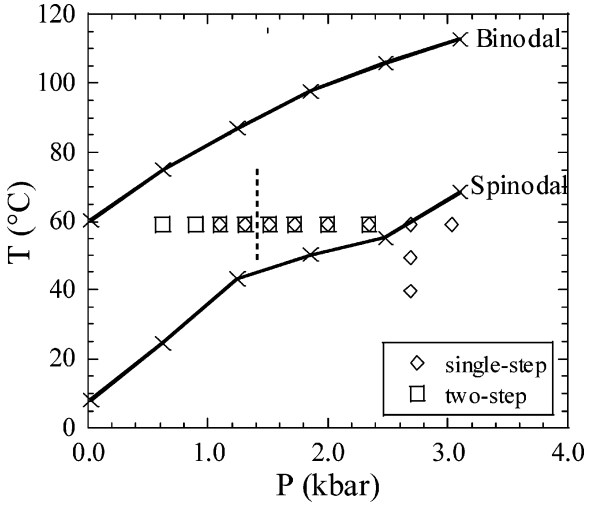

Figure 2. Temperature vs pressure phase diagram for the $\phi_{dPMB} = 0.20$ blend. Diamonds and squares represent single-step and two-step quench experiments, respectively. The dotted line demarcates pressures below which single-step quenches were ineffective on experimental time scales.

Table 1. Dependence of χ on Temperature at Selected Pressures (with a Reference Volume of 100 Å^3); $\chi = A + B/T + C/T^2$

P (kbar)	A	B (K)	C (K^2)
0.03	0.001 73	−1.154	271.85
0.62	0.001 81	−1.306	324.86
1.24	0.003 24	−2.477	569.47
1.86	0.001 58	−1.339	384.34
2.48	0.000 027 3	−0.225	192.80
3.10	0.001 98	−1.800	517.40

Table 2. Experimental Conditions and Corresponding Quench Depths

T (°C)	P (kbar)	κ	T (°C)	P (kbar)	κ
59	0.62	0.25	59	2.00	0.79
59	0.90	0.36	59	2.34	0.93
59	1.10	0.44	59	2.69	1.06
59	1.31	0.52	59	3.03	1.20
59	1.52	0.60	49	2.69	1.36
59	1.72	0.69	40	2.69	1.68

59, 49, or 40 °C. The SANS profile obtained prior to the pressure quench shows no evidence of phase separation. Nucleation was triggered by an isothermal pressure quench to the desired pressure. We define $t = 0$ as the time at which the pressure quench was initiated.

In Figure 3, we show the time-resolved SANS profiles obtained from single-step quenches at a variety of quench depths at $T = 59$ °C. Figure 3a shows data obtained at selected times for $t < 412$ min at $P = 1.31$ kbar, i.e., $\kappa = 0.52$. The SANS profiles are time-independent at all q values. Hence, we conclude that at $\kappa = 0.52$, which is roughly half way between the binodal and the spinodal, the nucleation barrier is too large for nucleation to be observed during experimental time scales. Figure 3b shows the results at a quench depth of $\kappa = 0.60$. Here, the intensity increases with time for small q (large structures) and is independent of time (after an initial relaxation period[32]) for large q (small structures). The division between these two regimes of behavior is marked by the critical scattering vector, q_c. This qualitative behavior is seen at all higher quench depths. In Figure 3c, we show data obtained just inside the classical spinodal at $\kappa = 1.06$. Scattering peaks are obtained outside the spinodal (Figure 3b), at the spinodal (Figure 3c), and inside the spinodal (not shown for brevity). For the $\kappa = 0.60$ quench $q_c = 0.046$ nm^{-1} (Figure 3b), while for the $\kappa = 1.06$ quench $q_c = 0.086$ nm^{-1}. We have established that q_c is a signature of the critical nucleus size, $R_c = 2\pi/q_c$. We use method 2 of ref 19 to determine q_c from the SANS data.

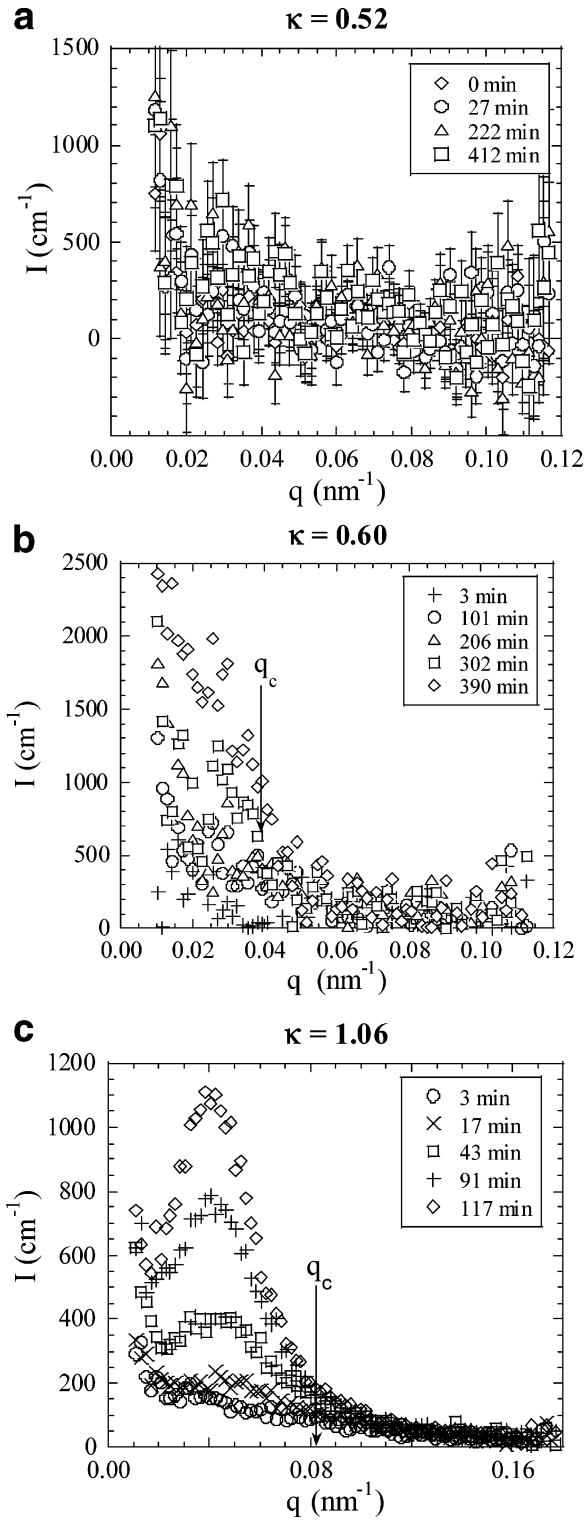

Figure 3. Time-dependent scattering intensity, I, vs q obtained for single-step quenches at 59 °C and (a) 1.31, (b) 1.52, and (c) 2.69 kbar. The arrows indicate the locations of q_c.

During the early stages of nucleation, the SANS intensity, I, increases linearly with time for $q < q_c$. During the later stages, the SANS intensity increases more rapidly and the I vs t curves are nonlinear. The time required to complete the early stage, τ_E, was determined using methods described in refs 19 and 33. All of the data shown in Figure 3 correspond to $t < \tau_E$.

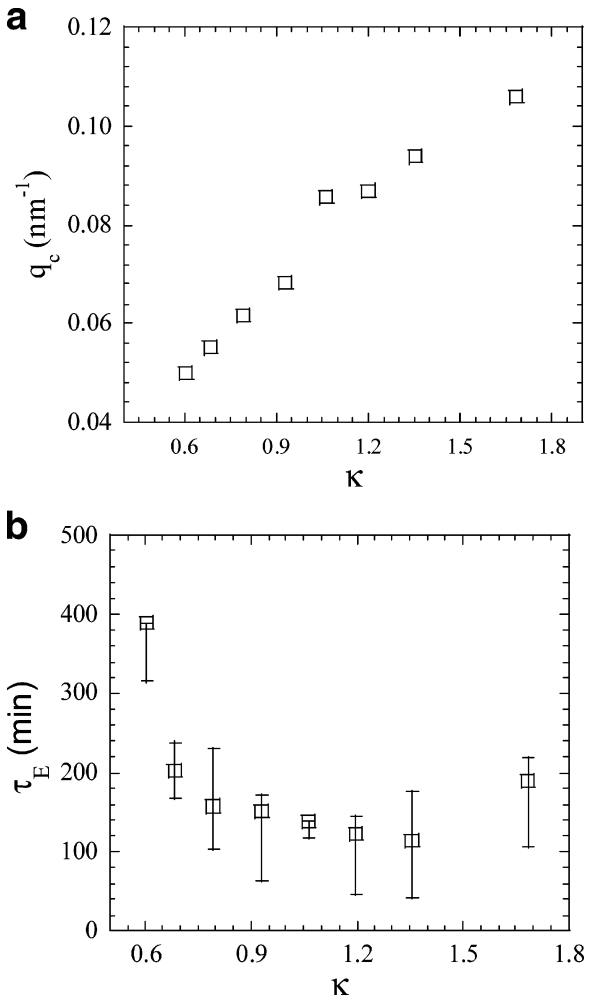

Figure 4. Variation of (a) the critical scattering vector, q_c, and (b) the time required to complete the early stage of nucleation, τ_E, with quench depth, κ, for single-step quenches.

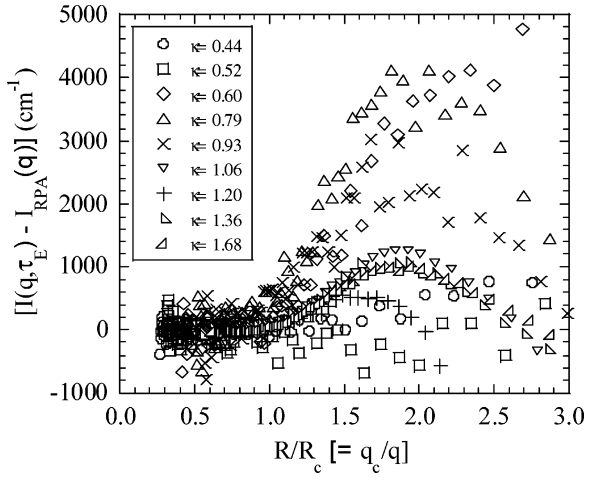

Figure 5. Excess scattering profile, $I(q;\tau_E) - I_{RPA}(q)$, obtained at the end of the initial stages of phase separation plotted vs the reduced nucleus size, R/R_c, for single-step quenches. R_c values for ineffective single-step quenches ($\kappa \leq 0.52$) were obtained subsequently from two-step quenches.

The analysis for determining q_c and τ_E was repeated for all of the single-step quenches that led to detectable phase separation, and the results are summarized in Figure 4. In Figure 4a we show the dependence of q_c on κ. It is evident that q_c is a smooth and monotonic function of κ in the range $0.60 \leq \kappa \leq 1.68$. Figure 4b shows the dependence of τ_E on κ.[34] At low

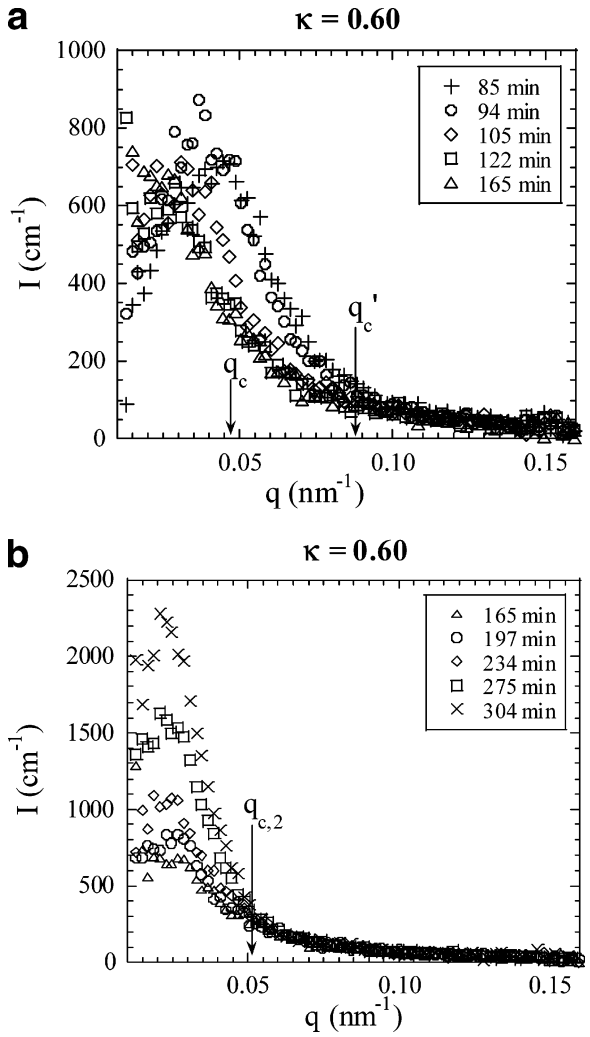

Figure 6. (a) Time dependence of the scattering intensity, I, vs q during the transient period (see text) of a two-step quench from $\kappa' = 1.06$ ($\tau_1 = 90$ min) to $\kappa = 0.60$. Plus symbols (+) represent the final scattering profile obtained at $\kappa' = 1.06$, and arrows indicate the critical scattering vectors, $q_c'(\kappa')$ and $q_c(\kappa)$, obtained from independent single-step quenches (Figure 3), (c) and (b), respectively. (b) Time dependence of the scattering intensity, I, vs q following the transient period of the two-step quench. The arrow indicates the critical scattering vector, $q_{c,2}$, obtained from data covering the time span shown.

quench depths, τ_E is expected to be large because the thermodynamic driving force for nucleation is low. At large quench depths, kinetic factors take over because molecular motion slows down due to reduced temperature and increased pressure. The nonmonotonic dependence of τ_E on κ is thus not surprising. Because of lack of knowledge of the effect of pressure on molecular motion, we are unable to separate the effect of thermodynamic and kinetic factors on τ_E. It is evident from Figure 4 that the combination of thermodynamic and kinetic factors makes studying phase separation kinetics at large quench depths relatively easy with our experimental system; the data in Figure 4 extend deep into the spinodal ($\kappa = 1.6$) where both q_c and τ_E are well within experimental resolution. On the other hand, our ability to explore small quench depths is limited by the steep increase in τ_E with decreasing quench depth (Figure 4b).

In Figure 5, we summarize the data obtained during the initial stages ($t < \tau_E$) of the single-step quench experiments by plotting $[I(q;\tau_E) - I_{RPA}(q)]$ vs R/R_c [$= q_c/q$]. $I_{RPA}(q)$ is calculated from eqs 1−3 using $\chi(T,P)$ values in accordance with Table 2. The χ parameters for the T and P values where phase separation is

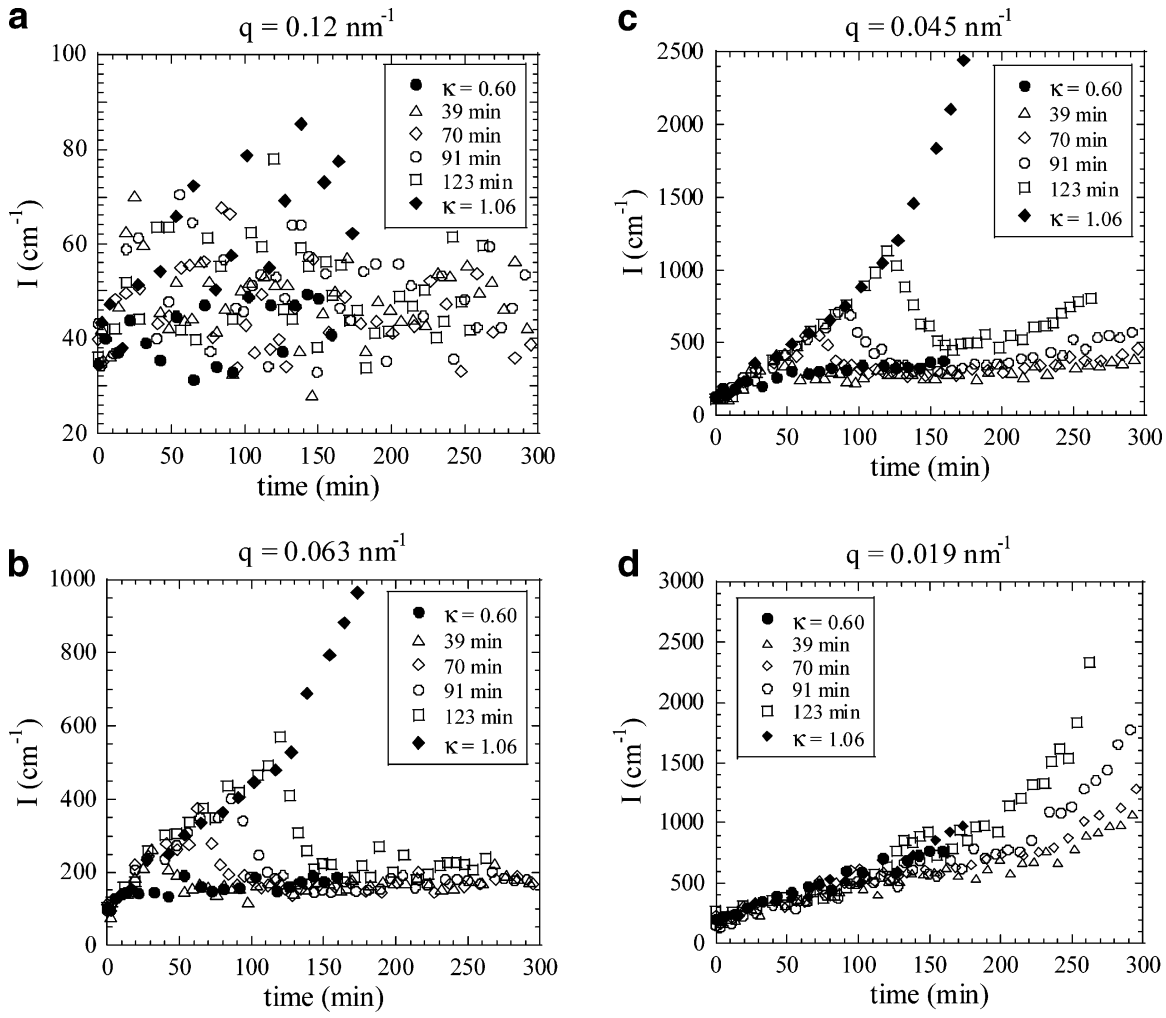

Figure 7. Time dependence of the scattering intensity I at (a) $q = 0.12$ nm^{-1}, (b) $q = 0.063$ nm^{-1}, (c) $q = 0.045$ nm^{-1}, and (d) $q = 0.019$ nm^{-1} for single-step quenches (solid symbols) and two-step quenches (open symbols), labeled according to τ_1, the time spent at $\kappa' = 1.06$ before quenching to $\kappa = 0.60$.

observed are thus extrapolations of data obtained from one-phase systems. The χ parameters determined from the present system are in good agreement with the previous studies.[31,35−37] We note in Figure 5 that for $R/R_c < 1.0$ values of $[I(q;\tau_E) - I_{RPA}(q)]$ scatter around zero; i.e., in this regime the scattering profiles obtained from our blends are identical to the RPA predictions for homogeneous blends. On the other hand, $[I(q;\tau_E) - I_{RPA}(q)]$ is significantly larger than zero for all of the quenches with $\kappa \geq 0.60$ (all viable quenches), when $R/R_c > 1.0$.

In Figure 6 we show $I(q;t)$ vs q at selected times for a two-step quench to $\kappa = 0.60$, following a single-step quench to $\kappa' = 1.06$ for $\tau_1 = 90$ min. The profile for $t = 85$ min is the last profile obtained during the first step at $\kappa' = 1.06$ and is similar to the $t = 91$ min profile shown in Figure 3c. In Figure 6a we show two critical scattering vectors q_c' and q_c; q_c' is the critical scattering vector for the first step (Figure 3c), and q_c is the critical scattering vector obtained from a single-step quench directly to $\kappa = 0.60$ (Figure 3b). The data in Figure 6a show that $I(q;t)$ in the range of scattering vectors, $q_c \leq q \leq q_c'$ decreases after the quench depth is changed from κ' to κ. This may be regarded as the *transient* stage where the nucleation process adjusts to the change in quench depth from κ' to κ. In Figure 6b we show data obtained after this transient stage is completed ($t = 165$ min). The time-dependent scattering profiles in Figure 6b are very similar to those obtained after a direct quench to $\kappa = 0.60$ (Figure 3b). The critical scattering vector for the second quench, which we call $q_{c,2}$, is indicated by the arrow in Figure 6b ($q_{c,2} = 0.052$ nm^{-1}). $q_{c,2}$ was obtained by the same methods that were used to determine q_c in Figure 3b (and all single-step quenches) except for the fact that the scattering profiles used in this analysis cover the time scale shown in Figure 6b; i.e., times after the transient stage are completed but before the completion of the early stage of nucleation. The value of $q_{c,2}$ obtained from the two-step quench is very similar to that obtained from the single-step quench to $\kappa = 0.60$, which gave $q_c = 0.050$ nm^{-1} (the average value for three separate single-step quenches to $\kappa = 0.60$).

We conducted a series of two-step quenches with $\kappa' = 1.06$ and $\kappa = 0.60$, with τ_1 varying from 39 to 123 min. The critical scattering vectors obtained from direct quenches to κ' and κ are $q_c' = 0.0854$ nm^{-1} and $q_c = 0.050$ nm^{-1}, respectively. A rich variety of time-dependent behaviors are seen, depending on the value of q, relative to q_c and q_c'. In Figure 7a, we show $I(t)$ for $q = 0.12$ nm^{-1}, which is typical of results obtained when $q > q_c'$. The scattering profiles in this regime are independent of time, i.e., neither the first nor the second quench has any effect on structures with $R < R_c'$. In Figure 7b, we show $I(t)$ for $q = 0.063$ nm^{-1}, which is typical of results obtained when $q_c < q < q_c'$. The filled symbols in Figure 7b show $I(t)$ obtained from direct quenches to κ' and κ. The open symbols represent two-step quench data, labeled according to their various age times, τ_1. Prior to the second quench, $I(t)$ follows the time dependence of $I(t)$ for a direct quench to κ'. This is clearly the

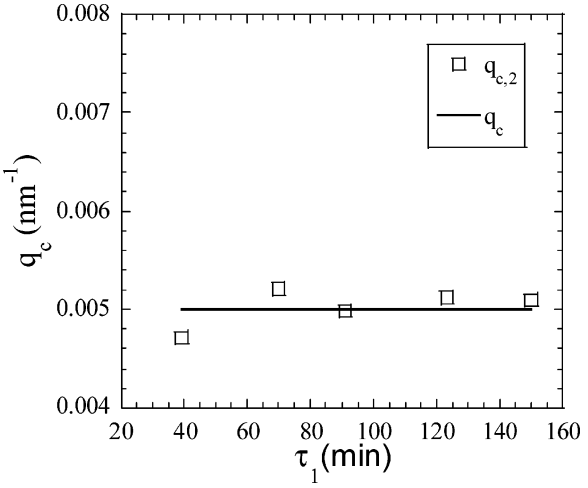

Figure 8. $q_{c,2}$ plotted as a function of τ_1 for a series of $\kappa' = 1.06$ and $\kappa = 0.60$ two-step quenches. The line represents q_c obtained from a direct quench to κ.

expected behavior because prior to the second quench, the sample was exposed to the same temperature and pressure history. After the second pressure quench to κ, we see a rapid decrease in intensity. When $I(t)$ reaches a value of about 150 cm^{-1}, this rapid decrease in intensity stops abruptly, and $I(t)$ follows a time-independent trajectory that is very similar to that obtained after a direct quench to κ. It is clear from Figure 7a,b that the effect of the perturbative quench to κ' has no discernible effect on scattering from the nucleating blend at a quench depth of κ, provided $q > q_c$. In Figure 7c, we show $I(t)$ for $q = 0.045$ nm^{-1}, which is slightly lower than q_c. This data set is similar to that shown in Figure 7b. For $\tau_1 \leq 91$ min, the second pressure quench to κ results in a decrease in $I(t)$ followed by a leveling-off at $I \approx 300$ cm^{-1} (Figure 7c). However, for the $\tau_1 = 123$ min case, $I(t)$ after the second quench stops decreasing when I reaches 500 cm^{-1} and then increases with time. Figure 7c shows the first evidence of departure of the $I(t)$ trajectories obtained from the two-step quenches, relative to those obtained from direct quenches. In Figure 7d we show $I(t)$ trajectories for $q = 0.019$ nm^{-1}, which is much lower than q_c. In this regime, we find that the second quench has little effect on $I(t)$ for $t < 200$ min. At later times the effect of the perturbative quench to κ' evident in Figure 7d. Faster increases in $I(t)$ are seen as τ_1 increases.

In Figure 8 we plot $q_{c,2}$ vs τ_1 obtained for the $\kappa' = 1.06$ and $\kappa = 0.60$ two-step quenches described in Figure 7. The line in Figure 8 represents q_c obtained from a direct quench to κ. It is clear that the perturbative quench has no effect on the determination of q_c for small enough τ_1. The agreement of q_c obtained from the single-step and two-step quenches and the decrease in scattering intensity in $q_c < q < q_c'$ window (Figures 7 and 8) provide substantive support for our proposed methodology for obtaining R_c from SANS experiments.

Our main goal in the next set of experiments was to obtain the critical nucleus size for the $\kappa \leq 0.52$ regime, where we were unable to observe any sign of nucleation kinetics within our experimental time window. In these experiments we fixed τ_1 to be about 100 min and $\kappa' = 1.06$ because our aim was to ensure that the perturbative quench had no effect on the critical nucleus size. Figure 9 shows the results of a two-step quench with $\kappa = 0.52$ and $\tau_1 = 90$ min. The transient stage data obtained right after the second quench, shown in Figure 9a, are very similar to the transient stage data in Figure 6a, obtained at $\kappa = 0.60$. The data obtained after completion of the transient stage at $\kappa = 0.52$, given in Figure 9b, show a $q < q_c$ regime where

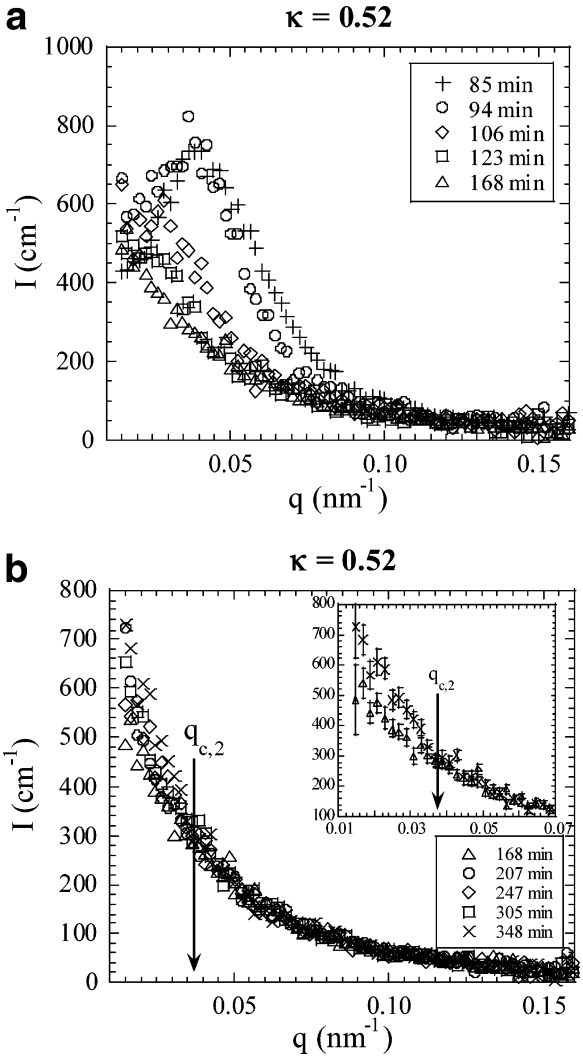

Figure 9. (a) Time dependence of the scattering intensity, I, vs q during the transient period of a two-step quench from $\kappa' = 1.06$ ($\tau_1 = 90$ min) to $\kappa = 0.52$. Plus symbols (+) represent the final scattering profile obtained at $\kappa' = 1.06$. (b) Time dependence of the scattering intensity, I, vs q following the transient period of the two-step quench. An arrow indicates the critical scattering vector, $q_{c,2}$, obtained from data covering the time span shown. Inset highlights the change in intensity occurring near $q_{c,2}$ for $168 < t < 348$ min.

$I(t)$ increases with time and a $q > q_c$ regime where $I(t)$ is independent of time. This enables determination of q_c at $\kappa = 0.52$. The inset in Figure 9b shows the changes that occur for $168 \leq t \leq 348$ min in the vicinity of $q \approx q_c$.

In parts a, b, and c of Figure 10, we show the post-transient stage data obtained from two-step quenches to $\kappa = 0.44$ ($\tau_1 = 109$ min), $\kappa = 0.36$ ($\tau_1 = 102$ min), and $\kappa = 0.25$ ($\tau_1 = 105$ min), respectively. We show only two scattering profiles—the scattering profile obtained at the end of the transient stage and the scattering profile obtained at the end of the experiment—and the values of $q_{c,2}$. In parts a and b of Figure 10 ($\kappa = 0.44$ and 0.36, respectively) we see a decrease in $q_{c,2}$ as the quench depth is reduced. In addition, the time required to observe $q_{c,2}$ increases dramatically. At $\kappa = 0.36$ we needed 935 min to obtain a significant increase in $I(t)$ at $q < q_c$ (Figure 10b). In Figure 10c, where we show the results for $\kappa = 0.25$, the scattering profiles until $t = 430$ min were time-independent for all q after completion of the transient stage. $\kappa = 0.36$ is thus the lowest quench depth accessible for study of nucleation kinetics with two-step quenches.

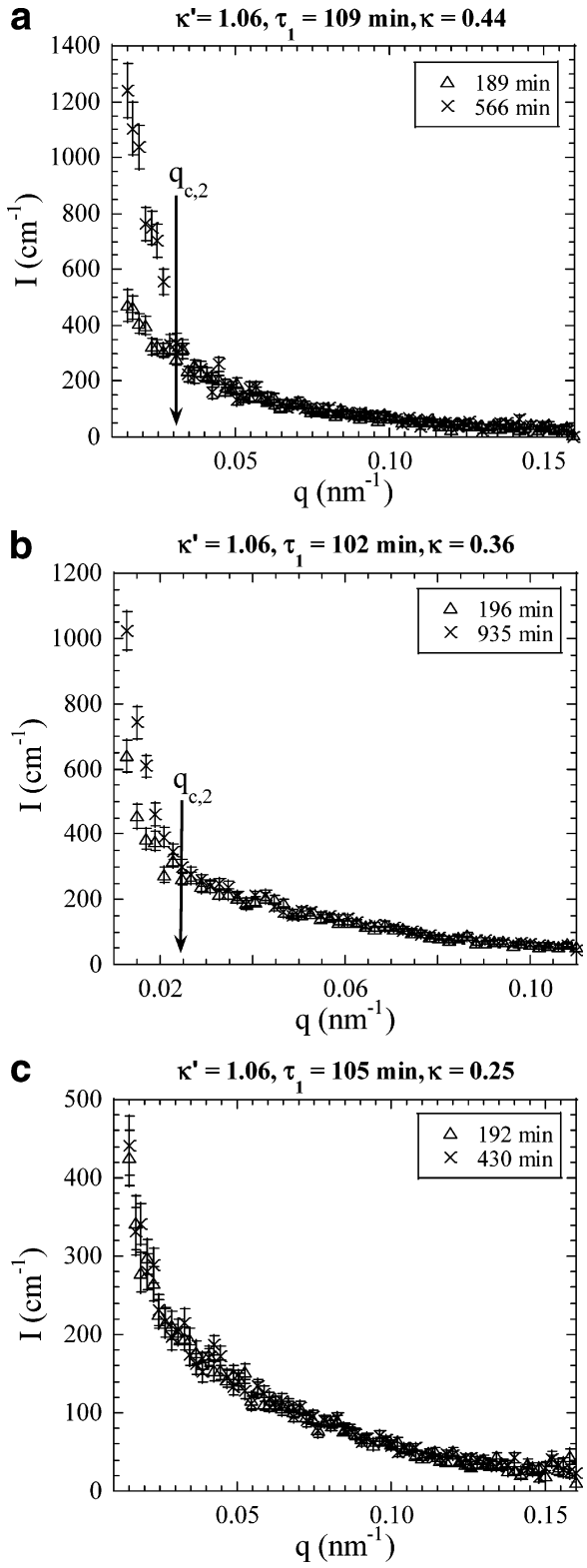

Figure 10. Scattering intensity, I, vs q for two-step quenches. The first profile represents the end of the transient period at κ, and the second profile represents the end of the nucleation experiment. Arrows show the locations of $q_{c,2}$ for (a) $\kappa' = 1.06$, $\tau_1 = 109$ min, $\kappa = 0.44$; (b) $\kappa' = 1.06$, $\tau_1 = 102$ min, $\kappa = 0.36$; and (c) $\kappa' = 1.06$, $\tau_1 = 105$ min, $\kappa = 0.25$, where $q_{c,2}$ could not be determined.

In Figure 5 we showed that the $I(q)$ of the blend for $q > q_c$ near the end of the early stage of phase separation for single-step quench experiments is described well by RPA. This is also true for two-step quench experiments. Figure 11 shows the excess scattering profile, $[I(q,\tau_{E,2}) - I_{RPA}(q)]$, vs R/R_c for all κ

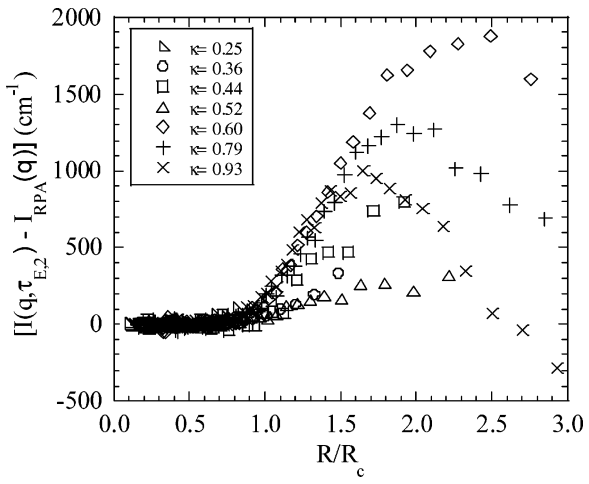

Figure 11. Excess scattering profile, $I(q;\tau_{E,2}) - I_{RPA}(q)$, obtained at the end of the initial stages of phase separation plotted vs the reduced nucleus size, R/R_c, for two-step quenches. The value of R_c for $\kappa = 0.25$ was estimated by extrapolating the trend of Figure 12b.

explored by two-step quenches.[38] Similar to the single-step quench experiments, $\tau_{E,2}$ is defined as the time for which the intensities begin to increase faster than their initial linear behavior (after the transient stage). Because of slow nucleation kinetics, $\tau_{E,2}$ was not observed for $\kappa \leq 0.60$. We thus use the last scattering profile obtained. The values of $\tau_{E,2}$, κ', and τ_1 for the profiles given in Figure 11 are presented in Table 3. Figure 11 clearly shows that the intensities in the $R < R_c$ regime, after the second quench in two-step quenches are described by RPA in spite of the increase of $I(q)$ in these systems after the first quench.

In Figure 12a, we show the dependence of the size of the critical nucleus on quench depth by plotting $R_c/R_g = 2\pi/(q_cR_g)$ vs κ. The results from direct and two-step quench experiments are given by open circles and solid triangles, respectively. For quench depths accessible to both types of experiments, the deviations in the measured R_c values are within experimental error. Our experiments cover an unprecedented range of quench depths, from $\kappa = 0.36$ to $\kappa = 1.5$. Throughout this regime we find that R_c is a monotonic and decreasing function of κ. Inside the spinodal ($\kappa > 1$), R_c has a weak dependence on κ. Within the classical metastable regime ($\kappa < 1$), R_c is a sensitive function of κ, increasing by a factor of 3 as κ decreases from 1 to 0.36. In Figure 12b, we plot R_g/R_c as a function of κ.[39] We find that R_g/R_c is a linear function of κ in the limit of low quench depths. Linear extrapolation of R_g/R_c vs κ data, shown by the solid line in Figure 12b, suggests that the critical nucleus size approaches infinity as κ approaches zero, in agreement with the classical theory. The data obtained from the two-step quenches are crucial for establishing quantification of nucleation characteristics at low values of κ. The least-squares fit through the $\kappa < 1$ data yields

$$R_g/R_c = 0.188\kappa \quad \text{(experiment)} \tag{6}$$

The Cahn−Hilliard theory of nucleation[1,3,40] predicts that the critical nucleus size diverges at both the binodal and the spinodal. The experimental behavior observed near the spinodal ($\kappa = 1$), seen in Figure 12a, is clearly not in agreement with this theory. We have discussed this discrepancy in previous studies,[10] and similar data are now being obtained in other systems such as protein solutions.[41] The present work enables the evaluation of classical nucleation theory in the vicinity of the binodal. According to the classical theory, the critical nucleus

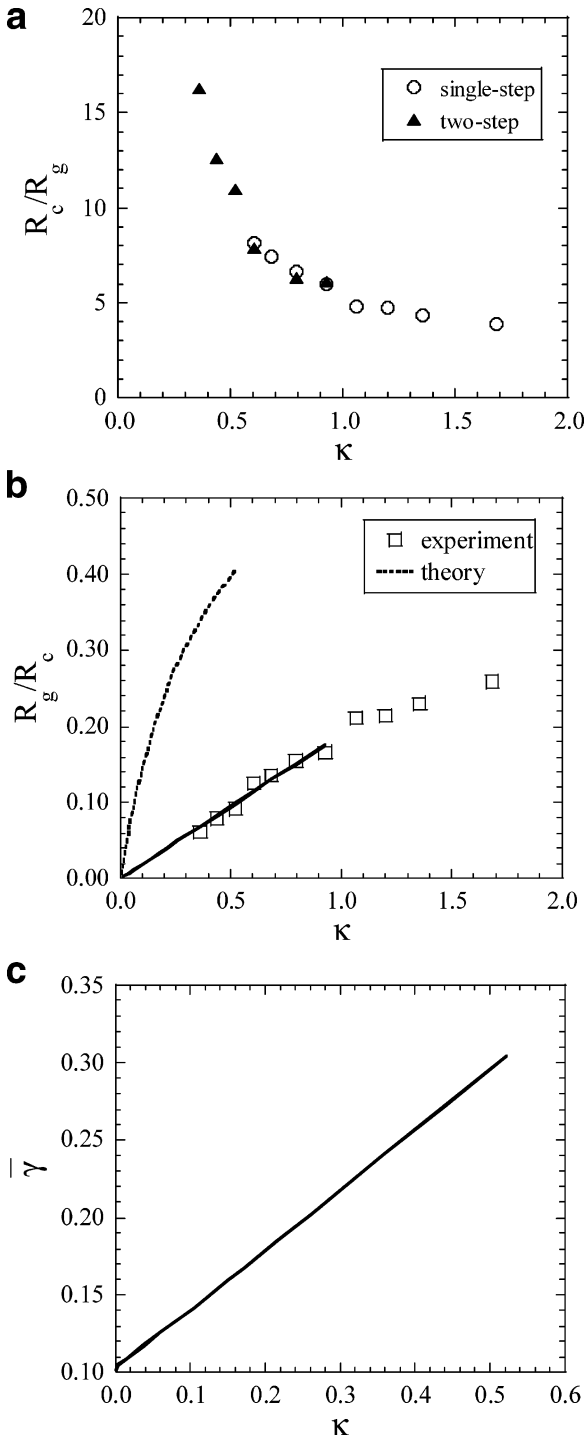

Figure 12. (a) The critical nucleus size (normalized by radius of gyration), R_c/R_g, plotted for single-step (open circles) and two-step (solid triangles) quenches. (b) R_g/R_c vs quench depth. The solid line is a linear fit to the experimental data, and the dotted line is the classical theory prediction. (c) Normalized interfacial tension, $\bar{\gamma} = \beta v_0 \gamma / R_{g1}$, plotted as a function of quench depth, κ.

is a spherical droplet of uniform composition that is in equilibrium with the metastable bulk phase (i.e., $\phi_{1,\text{nucleus}}$ is obtained by solving $\mu(\phi_{1,\text{nucleus}}) = \mu(\phi_{1,\text{bulk}})$). The free energy of formation of the nucleus, ΔG_N, of Figure 1 is given by $\Delta G_N(R) = -(4\pi R^3/3)\Delta G + 4\pi R^2\gamma$, and minimizing ΔG_N with respect to R leads to the expression for the critical radius, $R_c = 2\gamma/\Delta G$. Here γ is the interfacial tension, and ΔG, the free energy density difference between the nucleus and the bulk, is given by $\Delta G = (G_m(\phi_{1,\text{bulk}}) - G_m(\phi_{1,\text{nucleus}})) - \mu(\phi_{1,\text{bulk}})(\phi_{1,\text{bulk}} - \phi_{1,\text{nucleus}})$. Our approach for determining the classical prediction of R_c follows the treatment of Wood and Wang.[40] Since an expression for the interfacial tension as a function κ was not available for our system, we evaluated γ numerically using the self-consistent-field theory of Wood and Wang. Wood and Wang computed γ for a blend with $N_1/N_2 = R_{g,1}/R_{g,2} = 1.0$.[40] In our system $N_1/N_2 = 0.735$ and $R_{g,1}/R_{g,2} = 0.97$. The dependence of γ on κ for our system is presented in Figure 12c. The theoretical prediction of the classical theory of nucleation for R_g/R_c thus calculated is shown as a dotted curve in Figure 12b. The theoretically predicted critical nucleus size is about 4 times smaller than that determined experimentally. The significant difference between mean-field predictions and experiments seen at low values of κ in Figure 12b suggests that fluctuations play an important role during nucleation.

Table 3. Experimental Parameters for Figure 11[a]

κ	κ'	τ_1 (min)	$\tau_{E,2}$ (min)
0.25	1.06	105	(430)
0.36	1.06	102	(935)
0.44	1.06	109	(566)
0.52	1.06	90	(348)
0.60	1.06	90	(304)
0.79	1.06	91	164
0.93	1.06	91	138

[a] $\tau_{E,2}$ values in parentheses represent end of experiment times rather than true $\tau_{E,2}$ values.

Conclusions

The predictions of classical nucleation theory are most accurate close to the binodal. Unfortunately, both the critical nucleus size and the free energy barriers for the formation of the critical nucleus diverge at the binodal making experimentation difficult. Our previous attempts at measuring the critical nucleus size close to the binodal by a direct quench[10] were limited by the fact that nucleation could not be observed for quench depths $\kappa \leq 0.52$ (Figure 3a). At higher quench depths, the usual signatures of the early stages of nucleation in phase-separating polymer blends were observed (Figure 3b,c). In order to study nucleation at small quench depths, we used two-step quenches where a first perturbative deep quench allows for the formation of nuclei with relative ease, followed by a second quench to a lower quench depth. By first performing two-step quenches that terminated at locations already studied by a direct quench, we established the range of conditions under which the first quench does not affect R_c determined during the second quench (Figures 6−8). Data from the second quench were used to obtain the size of the critical nucleus at small quench depths (Figures 9 and 10). Our approach enables study of nucleation kinetics down to $\kappa = 0.36$. We find that $1/R_c$ scales linearly with quench depth, κ, in the low quench depth limit. The experimentally determined values of the critical nucleus are, however, substantially larger that those predicted by classical theories. We hope that our experiments will motivate the reexamination of nucleation theories and their application to polymer blends.

Acknowledgment is made to the donors of The Petroleum Research Fund, administered by the American Chemical Society, and the National Science Foundation (Grants CTS-0305711 and DMR-0514422) for support of this research. A.J.P. gratefully acknowledges the graduate researcher fellowship from Tyco Electronics. We acknowledge the support of the National Institute of Standards and Technology, U.S. Department of Commerce, in providing the neutron research facilities used in this work. This work utilized facilities supported in part by the National Science Foundation under Agreement DMR-0454672.

References and Notes

(1) Gibbs, J. W. *The Scientific Papers of J. Willard Gibbs*; Dover: New York, 1961.
(2) Debenedetti, P. G. *Metastable Liquids Concepts and Principles*; Princeton University Press: Princeton, NJ, 1996.
(3) Cahn, J. W.; Hilliard, J. E. *J. Chem. Phys.* **1959**, *31*, 688.
(4) Sur, A.; Lebowitz, J. L.; Marro, J.; Kalos, M. H. *Phys. Rev. B* **1977**, *15*, 3014.
(5) Langer, J. S.; Schwartz, A. J. *Phys. Rev. A* **1980**, *21*, 948.
(6) Binder, K. *J. Chem. Phys.* **1983**, *79*, 6387.
(7) Frankel, D.; ten Wolde, P. R. *Science* **1996**, *277*, 1975.
(8) Talanquer, V.; Oxtoby, D. W. *J. Chem. Phys.* **1998**, *109*, 223.
(9) Howland, R. G.; Wong, N. C.; Knobler, C. M. *J. Chem. Phys.* **1980**, *73*, 522.
(10) Balsara, N. P.; Rappl, T. J.; Lefebvre, A. A. *J. Polym. Sci., Part B: Polym. Phys.* **2004**, *42*, 1793−1809.
(11) Strobl, G. *Eur. Phys. J. E* **2000**, *3*, 165.
(12) Gasser, U.; Weeks, E. R.; Schoefield, A.; Pusey, P. N.; Weitz, D. A. *Science* **2001**, *292*, 258.
(13) Debenedetti, P. G. *Nature (London)* **2006**, *441*, 168−169.
(14) Pan, A. C.; Rappl, T. J.; Chandler, D.; Balsara, N. P. *J. Phys. Chem. B* **2006**, *110*, 3692−3696.
(15) More precise definitions of quench depth require specifying the phase transition of interest, and the explicit definition of quench depth for our system is given below.
(16) Balsara, N. P.; Lin, C.; Hammouda, B. *Phys. Rev. Lett.* **1996**, *77*, 3847−3850.
(17) Lefebvre, A. A.; Lee, J. H.; Jeon, H. S.; Balsara, N. P.; Hammouda, B. *J. Chem. Phys.* **1999**, *111*, 6082−6099.
(18) Lefebvre, A. A.; Lee, J. H.; Balsara, N. P.; Hammouda, B. *J. Chem. Phys.* **2002**, *116*, 4777−4781.
(19) Lefebvre, A. A.; Lee, J. H.; Balsara, N. P.; Vaidyanathan, C. *J. Chem. Phys.* **2002**, *117*, 9063−9073.
(20) Lefebvre, A. A.; Lee, J. H.; Balsara, N. P.; Vaidyanathan, C. *J. Chem. Phys.* **2002**, *117*, 9074−9083.
(21) Balsara, N. P.; Jonnalagadda, S. V.; Lin, C. C.; Han, C. C.; Krishnamoorti, R. *J. Chem. Phys.* **1993**, *99*, 10011−10020.
(22) Lin, C. C.; Jonnalagadda, S. V.; Balsara, N. P.; Han, C. C.; Krishnamoorti, R. *Macromolecules* **1996**, *29*, 661−669.
(23) Fetters, L. J.; Lohse, D. J.; Colby, R. H. In *Physical Properties of Polymers Handbook*; Mark, J. E., Ed.; AIP Press: Woodbury, NY, 1996; pp 335−340.
(24) de Gennes, P. G. *Scaling Concepts in Polymer Physics*; Cornell University Press: Ithaca, NY, 1979.
(25) Lefebvre, A. A.; Lee, J. H.; Balsara, N. P.; Hammouda, B. *Macromolecules* **2000**, *33*, 7977−7989.
(26) Staverman, A. J.; Van Saten, J. H. *Recl. Trav. Chim.* **1941**, *60*, 76.
(27) Flory, P. J. *J. Chem. Phys.* **1942**, *10*, 51.
(28) Huggins, M. L. *J. Phys. Chem.* **1942**, *46*, 151.
(29) It has recently been shown that a true off-critical thermodynamic spinodal does not exist and instead the use of a "pseudo-spinodal" is recommended.[30] However, for the purpose of this paper, the term "spinodal" is used to denote the mean-field spinodal.
(30) Wang, Z.-G. *J. Chem. Phys.* **2002**, *117*, 481−500.
(31) Lefebvre, A. A.; Balsara, N. P.; Lee, J. H.; Vaidyanathan, C. *Macromolecules* **2002**, *35*, 7758−7764.
(32) There is always an initial relaxation period, even in the case of quenches made within the one-phase region, as the scattering profile goes from the RPA-predicted profile at the initial χ to that at the final χ.
(33) τ_E values are 390, 139 min for $\kappa = 0.6, 1.06$.
(34) The values of τ_E presented in this paper were obtained by a procedure similar to that given in ref 19. $S_2(t)$ is defined as the average of I up to time t plus 2 times the standard deviation in the data set up to time t. The earliest data point at which the intensity at the subsequent time point is greater than $S_2(t)$ is called τ_E. The lower and upper limits of the error in τ_E are defined to be $\tau_{E,min}$ and $\tau_{E,max}$, respectively. We use the time-dependent trajectories of $I_{min}(t) = I(t) - I_{err}(t)/2$ and $I_{max}(t) = I(t) + I_{err}(t)/2$ to obtain these limits. $S_{2,min}(t)$ is calculated for a data set using $I_{min}(t)$, and the earliest point at which $I_{max}(t)$ at the subsequent time point is greater than $S_{2,min}(t)$ gives $\tau_{E,min}$. Similarly, $S_{2,max}(t)$ is calculated for a data set using $I_{max}(t)$, and the earliest point at which $I_{min}(t)$ at the subsequent time point is greater than $S_{2,max}(t)$ gives $\tau_{E,max}$.
(35) Balsara, N. P.; Lefebvre, A. A.; Lee, J. H.; Lin, C. C.; Hammouda, B. *AIChE J.* **1998**, *44*, 2515−2519.
(36) Lefebvre, K. K.; Lee, J. H.; Balsara, N. P.; Hammouda, B.; Krishnamoorti, R.; Kumar, S. *Macromolecules* **1999**, *32*, 5460−5462.
(37) The agreement is within 10% in all cases.
(38) R_c for $\kappa = 0.25$ was estimated by extrapolating the trend in Figure 12b.
(39) For κ values where R_c was measured by both single-step and two-step quenches, the average of the two values is used.
(40) Wood, S. M.; Wang, Z.-G. *J. Chem. Phys.* **2002**, *116*, 2289−2300.
(41) Shah, M.; Galkin, O.; Vekilov, P. G. *J. Chem. Phys.* **2004**, *121*, 7505−7512.
(42) *Disclaimers*: (1) The experiments described here were performed by T. J. Rappl with the assistance and guidance of one of the coauthors (N.P.B.). (2) Certain commercial equipment, instruments, or materials (or suppliers, or software) are identified in this paper to foster understanding. Such identification does not imply recommendation or endorsement by the National Institute of Standards and Technology, nor does it imply that the materials or equipment identified are necessarily the best available for the purpose.

MA061947+